Optoelectronic Materials ISSN 2377-4738 *Optoelectron. Mater.* ***1*** *(2016) 63–67*

Impact of adding boric acid in the starting materials on the crystal structure and electronic structure of Dy doped $SrAl_2O_4$

Bao-gai Zhai, Ming Yu Li, Yuan Ming Huang*

School of Mathematics and Physics, Changzhou University, Jiangsu 213164, China
(*Received 1 December 2016; accepted 25 December 2016*)

Dy^{3+} doped $SrAl^2O_4$ nanoparticles were synthesized via the sol-gel combustion technique. The impacts of the addition of different amount of H_3BO_3 into the starting material on the crystal structure, photoluminescent properties and electronic structures of Dy^{3+} doped $SrAl_2O_4$ were investigated by X-ray diffractometer and spectrophotometer, respectively. The electronic structures of $SrAl_{2-\delta}B_\delta O4$ (δ = 0–1) were derived with first-principles density functional calculations in the framework of meta generalized gradient approximation. It is found that the addition of H_3BO_3 into the starting materials has significant effect on the crystal structure of Dy^{3+} doped $SrAl_2O_4$. Crystal contraction has been observed as more and more H_3BO_3 is added into the starting materials. As a contrast, the addition of different amount of H_3BO_3 has limited effects on the photoluminescent properties and electronic structures of Dy^{3+} doped $SrAl_2O_4$. No defect energy levels are introduced into the bandgap of $SrAl_2O_4$ while the bandgap value of $SrAl_{2-\delta}B_\delta O_4$ decreases from 7.5603 to 7.0641 eV as δ increases from 0 to 1.

Keywords: Strontium aluminate; Boric acid; Crystal structure; Photoluminescence; Electronic structures

1. Introduction

Recently Dy^{3+} doped $SrAl_2O_4$ (DSAO) has attracted attention because of the observation of green afterglow from DSAO in the absence of Eu^{2+} ions as the green luminescence center [1-5]. One of the most prominent characteristics of DSAO is that green afterglow can be prolonged from a couple of minutes to hours by adding 10 mol% boric acid (H_3BO_3) into the starting material for the combustion synthesis [4]. As reported in the literature, a variety of boron sources (i.e., $B(OCH_3)_3$ [6], B_2O_3 [7,8], H_3BO_3 [9,10]) were added into the starting materials to synthesize $SrAl_2O_4:Eu^{2+},Dy^{3+}$, $SrAl_2O_4:Eu^{2+}$ and $CaAl_2O_4:Eu^{2+},Nd^{3+}$ in the hope of forming proper trap levels in the phosphors. These studies suggest that the incorporation of boron dopant into the phosphors can affect the crystal structures and the afterglow of the phosphors. For example, Haranath *et al.* reported that H_3BO_3 acted as a fluxing agent in promoting formation of the required crystalline phase in the lower concentration range (<10 mol%) whereas it behaved as one of the precursor materials for formation of aluminoborate complexes in the higher (>10 mol%) range [10]. In our previous report, we demonstrated that the addition of H_3BO_3 into the starting materials for the synthesis of DSAO can dramatically alter the afterglow of the phosphor [4]. However, it is still not known how both the crystal structure and the electronic structure of DSAO evolve with the boron concentration.

In this paper, we report the evolution of crystal structure, photoluminescence (PL) and electronic structure of DSAO with the H_3BO_3 concentration in the starting materials. It is found the the crystal structure of DSAO changes with H_3BO_3 concentration, but the PL and electronic structures of DSAO, the latter of which are derived through first-principles calculations by employing meta generalized gradient approximation (meta GGA) in the density functional theory (DFT) [11,12], are not so much.

*Corresponding author. Email: dongshanisland@126.com

2. Materials and method

DSAO nanoparticles were prepared by the sol-gel combustion method [1-5]. All reagents were provided by Sinopharm Chemical Reagents Co., Ltd. (Shanghai, China). The purity of dysprosium oxide (Dy_2O_3) was 99.99% while all other reagents were in analytical grade. Strontium nitrate (0.2 mol), aluminum nitrate (0.4 mol), urea (6 mol), dysprosium oxide (0.0016 mol) and a specific amount of H_3BO_3 were dissolved in distilled water (600 mL) to form a transparent solution under the vigorous stirring of a magnetic bar. The solution was stored at room temperature for a couple of days. The molar ratio of urea : strontium nitrate : aluminum nitrate was 30:1:2. In the starting material, the molar ratio of Dy^{3+} ions to $Sr(NO_3)_3$ was fixed to be 1.6%, but that of $H3BO_3$ to $Sr(NO_3)_3$ varied from 0 to 0.18. An alumina crucible was filled with 30 ml of the sol-gel, and then it was transferred into an air-filled furnace for sol-gel combustion. The sol-gel firing temperature in the furnace was fixed at 600^o C.

X-ray diffraction (XRD) patterns were recorded on an X-ray diffractometer (D/max 2500 PC, Rigaku Corporation, Japan) using Cu Kα radiation (λ=1.5405 Å). The PL spectra of the phosphors were taken at room temperature on a spectrophotometer (Tianjin Gangdong Inc., China). A grating with 1200 grooves/mm was installed into the photospectrometer, the spectral resolution of the photospectrometer was around 0.2 nm at 500 nm. The excitation source for the PL measurement was the 325 nm emission line from a helium-cadmium laser (Kimmon Koha Co. Ltd., Japan). Other parameters on the instrumentation were available elsewhere [1 – 5].

First-principles DFT calculations of the band structures of $SrAl_2O_4$ with different B doping concentrations were performed using the DFT module of the Quantumwise Atomistix ToolKit 11.8 package. The exchange-correlation functional was treated within the meta GGA scheme [11,12]. The exchange potential in the meta GGA scheme was described by the modified Becke and Johnson exchange potential (i..e., TB09LDA) [12]. The Monkhorst-Pack scheme k-points grid sampling was

set at 5×5×5 for the Brillouin zone. There were 4 Sr, 8 Al and 16 O sites in the unit cell of SrAl2O4. The initial structural data of $SrAl_2O_4$ were taken from Inorganic Crystal Structure Database (ICSD no 26466). The values of a = 0.5163 nm, b = 0.8447 nm, c = 0.8816 nm and β = 93.42 were used in present work. The considered electronic configurations were $4s^24p^65s^2$ for Sr, $2s^22p^4$ for O and $3s^23p^1$ for Al. Double zeta double polarized basis sets were chosen for each element. The mesh cut-off energy was set to be 125 Hartree.

3. Results and discussions

Fig. 1 represents the XRD curves of the DSAO prepared with different H_3BO_3 concentrations in the starting materials. Despite the variation in the amount of H_3BO_3 flux, all of the samples show the typical X-ray patterns of $SrAl_2O_4$ crystal phase of the monoclinic $SrAl_2O_4$. The XRD data of the standard monoclinic $SrAl_2O_4$ (JCPDS card No. 34-0379) are depicted at the bottom of Fig. 1 for comparison. The lattice parameters of the standard monoclinic $SrAl_2O_4$ are known to be a = 0.8442 nm, b = 0.8822 nm, c = 0.5161 nm and β = 93.415°. The volume of the unit cell is 0.3837 nm^3 for the standard monoclinic SrAl2O4. We can see in Fig. 1 that the three dominant peaks in the XRD curve are located at 28.386, 29.275 and 29.922°, which can be assigned to the diffraction from crystallographic planes ($\bar{2}11$), (200) and (211) of $SrAl_2O_4$, respectively [1-5]. We have noticed the appearance of two diffraction peaks at around 25.1 and 25.7° in the XRD curves. H_3BO_3, which is often used as a fluxing agent in promoting formation of the required crystalline phase, can also behave as one of the precursor materials for the formation of aluminoborate complexes.

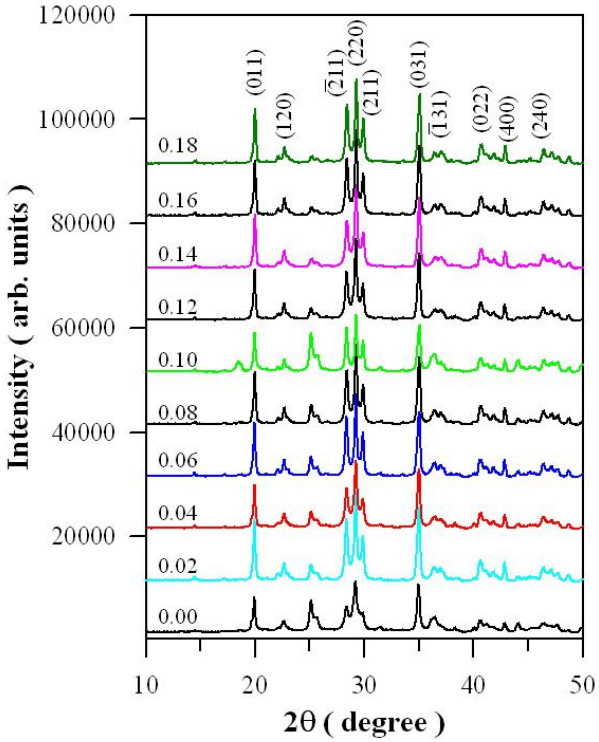

Fig. 1 XRD curves of the DSAO:B_x (x = 0.00–0.18) prepared with different H_3BO_3 concentrations in the starting materials.

Some authors attributed the two diffraction peaks to the formation of aluminoborate complex in the combustion synthesis due to the addition of H_3BO_3 [7]. However, such two peaks are present in the XRD curve even when no H_3BO_3 is added into the starting materials. So the two peaks, which are irrelevant to the formation of aluminoborate complexes, should have direct relation to the formation of secondary phase of aluminate, i.e., another type of strontium aluminate phase such as $SrAl_4O_7$ or $Sr_2Al_2O_7$. As more and more H_3BO_3 is added into the starting materials, the XRD intensities of the two diffraction peaks are weakened, indicating that the addition of H_3BO_3 promotes the formation of the required crystalline phase, i.e., the monoclinic $SrAl_2O_4$.

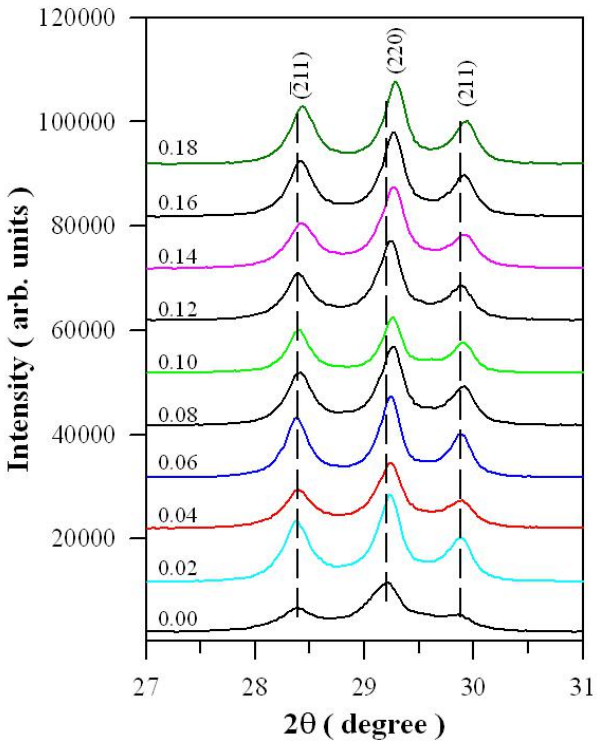

Fig. 2 Evolution of zoomed XRD curves of the DSAO with the concentration of H_3BO_3 in the starting materials.

Figure 2 displays the evolution of zoomed XRD curves of the DSAO with the concentration of H_3BO_3 in the starting materials. As can be seen in Fig. 2, the X-ray diffraction peaks of the 211, 220 and 211 diffraction planes are shifted to higher angles as the concentration of H_3BO_3 increases. This results in lattice contraction according to the Bragg's law, which gives the angles for coherent and incoherent scattering from a crystal lattice. Yu and Kim reported the contractions of lattice parameters a and c of Eu^{2+} and Dy^{3+} co-doped $SrAl_2O_4$ crystals with increasing B_2O_3 concentration [7]. From the observations in Fig. 2, adding H_3BO_3 into the starting materials causes some changes in the crystal structure of DSAO. In the monoclinic $SrAl_2O_4$, a three-dimensional network is formed by corner-sharing AlO_4 tetrahedra, and the Sr^{2+} ions are located along the channels in the a- and c-directions. Such a tridymite structure in monoclinic $SrAl_2O_4$ gives easy channels for Dy^{3+} ion to substitute the Sr^{2+} in the host. The ionic radius of Dy^{3+} is around 91.2 pm whereas that of Sr^{2+} is 118 pm. Thus the substitution of Sr^{2+} sites in $SrAl_2O_4$ with Dy^{3+} ions can result in lattice

contraction. However, this case can be excluded in our samples since the concentration of Dy^{3+} ions in the starting materials is fixed to be 1.6 mol %. There is still one possible reason to be responsible for the lattice contraction, which is the differences in ionic radii in B^{3+} and Al^{3+} ions. It is known that the ionic radius of B3+ ion (27 pm) is smaller than that of Al^{3+} ion (53.5 pm). Therefore, the recorded lattice contraction suggests that more and more B^{3+} atoms substitute Al^{3+} sites in the lattice of $SrAl_2O_4$. These changes in lattice parameters reflect the strain in the crystals. There are generally two kinds of strains in a crystal: a heterogeneous strain (micro strain) and a uniform strain (macro strain). The heterogeneous strain means that lattice parameters vary from place to place in the crystal. The existence of the strain can be evaluated by XRD's peak broadening analysis. The uniform strain means that all of crystal lattice is uniformly distorted by a stress, and can be evaluated from peak shift analysis. The analysis of the peak shift of the XRD peaks, which can be used to certify the nature of the uniform strain in crystals, is not given here.

Figure 3 represents the evolution of the PL spectra of DSAO with the concentrations of H_3BO_3 in the starting materials. As can be seen in Fig. 3, the PL spectrum of the original DSAO consists of a broad PL band centered at about 400 nm and the two characteristic emission bands of Dy^{3+} ions peaking at 480 and 575 nm, respectively. On one hand, the broad PL spectrum can be attributed to defect emissions of host $SrAl_2O_4$ when excited by 325 nm. It is known that perfect monoclinic $SrAl_2O_4$ crystal, whose Eg is around 6.52 eV, should exhibit no visible emissions under the 325 nm excitation. Intrinsic defects such as oxygen vacancies are supposed to be responsible for the broadband emission in Fig. 3 [5]. On the other hand, the two narrow PL bands centered at 480 and 575 nm, which can be discernible in Fig. 3(a), are the well known blue and yellow emissions of Dy^{3+}. Free Dy^{3+} ion has 9 electrons in the 4f state, its spin-orbit coupling gives rise to the formation of $^{2S+1}L_J$ configurations, each of which is (2J+1) – fold degenerate. So the spectral terms of the six multiplets of the ground state of Dy^{3+} can be denoted as ^6H_J where J = 15/2, 13/2, 11/2, 9/2, 7/2 and 5/2, respectively. In a similar way, the spectral term of the lowest energy excited state of Dy^{3+} ion is determined as $^4F_{9/2}$. When the Dy^{3+} ions are excited to any level above the 4F9 state, there is a fast non-radiative multiphonon relaxation to this level, and then the excited Dy^{3+} ions at $^4F_9$ level is relaxed by radiative $^4F_9 \rightarrow {}^6H_J$ transitions. As a result, the transition $^4F_{9/2} \rightarrow {}^6H_{15/2}$ yields the blue PL band centered at 480 nm whereas the transition $^4F_{9/2} \rightarrow {}^6H_{13/2}$ leads to the yellow PL band centered at 575 nm. Consequently, the two narrow PL bands in Fig. 3 can be assigned to the characteristic emissions of Dy^{3+} due to its $^4F_{9/2} \rightarrow {}^6H_{15/2}$ and $^4F_{9/2} \rightarrow {}^6H_{13/2}$ transitions. Evidence for such assignment can also be evidenced by other reports documented in the literature [1–5]. It is obvious that both the broadband emission of the host and the characteristic emissions of Dy^{3+} show little dependence on the H_3BO_3 concentration.

As documented in the literature, the transition $^4F_{9/2} \rightarrow {}^6H_{15/2}$ ($\Delta L = 2$ and $\Delta J = 3$) is magnetic dipole allowed one whereas the transition $^4F_{9/2} \rightarrow {}^6H_{13/2}$ is identified as a hypersensitive electric dipole transition ($\Delta L = 2$ and $\Delta J = 2$) of Dy^{3+} [13]. As a result, the emission intensity of the transition $^4F_{9/2} \rightarrow {}^6H_{15/2}$ is less sensitive to the local crystal field around Dy^{3+} in the host but the emission intensity of the transition $^4F_{9/2} \rightarrow {}^6H_{13/2}$ is highly influenced by the local crystal field around Dy^{3+} in the host environment. The luminescence intensity ratio (R) between the electric ($^4F_{9/2} \rightarrow {}^6H_{13/2}$) and magnetic ($^4F_{9/2} \rightarrow {}^6H_{15/2}$) dipole transitions provides valuable information on the local surroundings of the Dy^{3+} ion in the host. Generally, the value of R is proportional to the $Dy^{3+} - O^{2-}$ covalence, the higher the R value is, the lower the symmetry around Dy^{3+} ion is. So the difference in R reflects the difference in the local surroundings of the Dy3+ ion. In other words, the host matrices become less symmetrical and the intensity of the electric dipole transition becomes more intense when the interaction of the rare earth ion with its host material is stronger. Therefore, the changes in the lattice parameters suggest some changes in the crystal environment around Dy^{3+} ions in $SrAl_2O_4$.

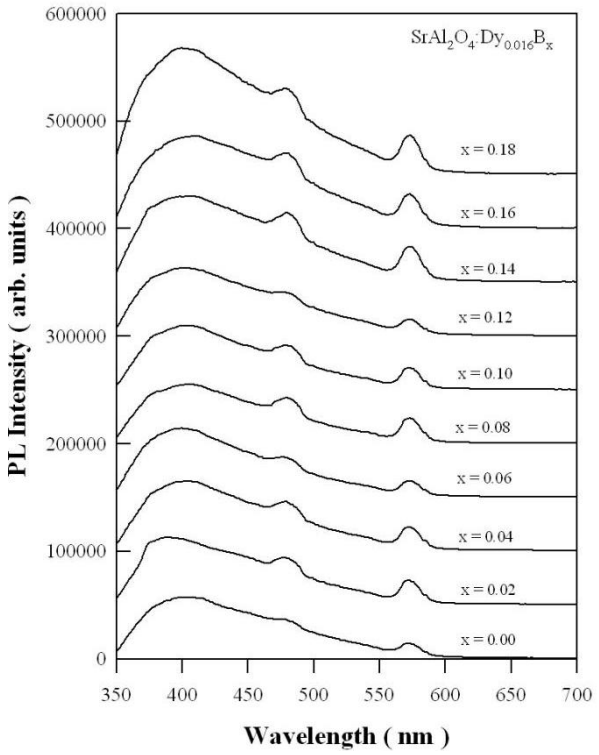

Fig. 3 Evolution of the PL spectra of DSAO with the concentrations of H_3BO_3 in the starting materials.

Figure 4 represents the calculated bandstructures of $SrAl_2O_4$ (*a*), $SrAl_{1.75}B_{0.25}O_4$ (*b*), $SrAl_{1.50}B_{0.50}O_4$ (*c*), $SrAl_{1.25}B_{0.75}O_4$ (*d*), $SrAl_{1.00}B_{1.00}O_4$ (*e*). The most striking feature of Fig. 4(a–e) is that their bandstructures are quite similar to each other. In each calculated bandstructure, the minimal-energy state in the conduction band is located at Gamma point whereas the maximal-energy state in the valence band is located at B point, so the boron doped $SrAl_2O_4$ is an indirect bandgap material since the k-vectors of the minimal-energy state in the conduction

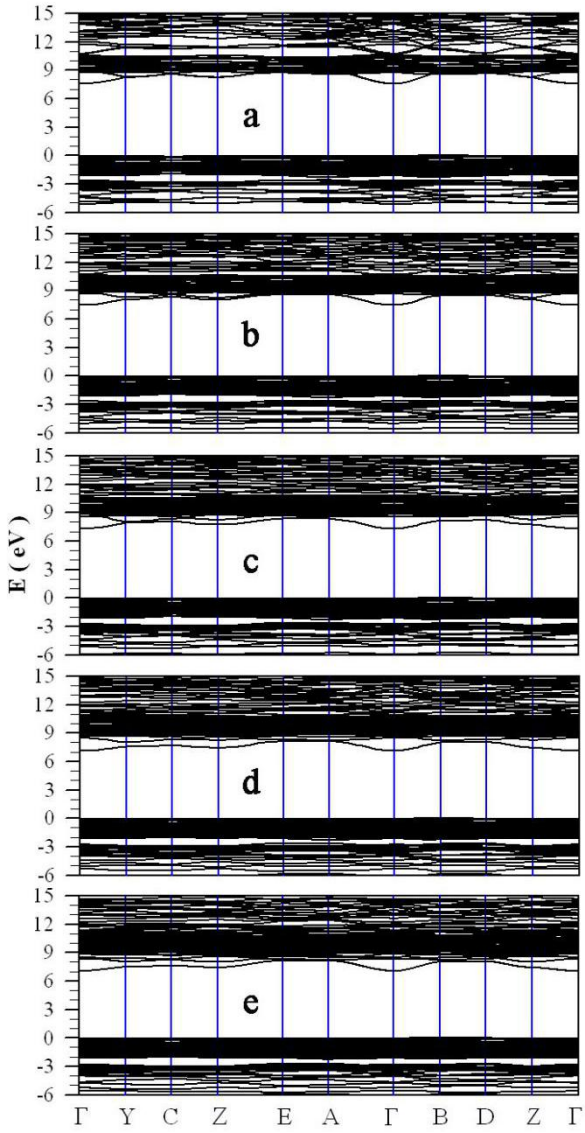

Fig. 4 Calculated bandstructures of $SrAl_2O_4$ (*a*), $SrAl_{1.75}B_{0.25}O_4$ (*b*), $SrAl_{1.50}B_{0.50}O_4$ (*c*), $SrAl_{1.50}B_{0.50}O_4$ (*d*), $SrAl_{1.50}B_{0.50}O_4$ (*e*).

band and the maximal-energy state in the valence band are different in the Brillouin zone. In an indirect gap, a photon cannot be emitted because the electron must pass through an intermediate state and transfer momentum to the crystal lattice. The calculated indirect bandgap value is 7.5603 eV for $SrA_{l2}O_4$, 7.4695 eV for $SrAl_{1.75}B_{0.25}O_4$, 7.2987 eV for $SrAl_{1.50}B_{0.50}O_4$, 7.1169 eV for $SrAl_{1.25}B_{0.75}O_4$, and 7.0641 eV for $SrAl_{1.00}B_{1.00}O_4$. It is clear that the indirect bandgap value decreases with the increase in the boron doping concentration. In our previous work, we carried out first-principles DFT calculations of the band structures of $SrAl_2O_4$, ZnO, $ZnMoO_4$ with different kinds of intrinsic defects [14 – 17]. What is the reason behind decreasing bandgap on boron doping? It depends on where the Fermi level of the dopant really is, which in turn gives rise to band tails. This leads to the effective decrease or increase in the band gap. An over simplified example would be when the dopant material has a conduction band or valence band energy between the conduction band and valence band of the host material, it would create a band tail and effectively lower the band gap. Thus, Fig. 4 has demonstrated that the addition of different amount of H3BO3 has limited effects on the electronic structures of DSAO. No defect energy levels are introduced into the bandgap of SrAl2O4 while the bandgap value of $SrAl_{2-\delta}B_\delta O_4$ decreases from 7.5603 to 7.0641 eV as δ increases from 0 to 1.

Figure 5 depicts the calculated densities of states of $SrAl_2O_4$ (*a*), $SrAl_{1.75}B_{0.25}O_4$ (*b*), $SrAl_{1.50}B_{0.50}O_4$ (*c*), $SrAl_{1.25}B_{0.75}O_4$ (d), $SrAl_{1.00}B_{1.00}O_4$ (e). It is clear that the density of state plots in Fig. 5 resemble each other although their bandgap values are different. We can see the slightly down shift in the conduction band as the concentration of boron dopant increases. In solid-state and condensed matter physics, the density of states of a system describes the number of states per interval of energy at each energy level available to be occupied. Unlike isolated systems such as atoms or molecules in the gas phase, the density distributions are not discrete but continuous. A high density of state at a specific energy level means that there are many states available for occupation. A density of state of zero means that no states can be occupied at that energy level. In general a density of state is an average over the space and time domains occupied by the system.

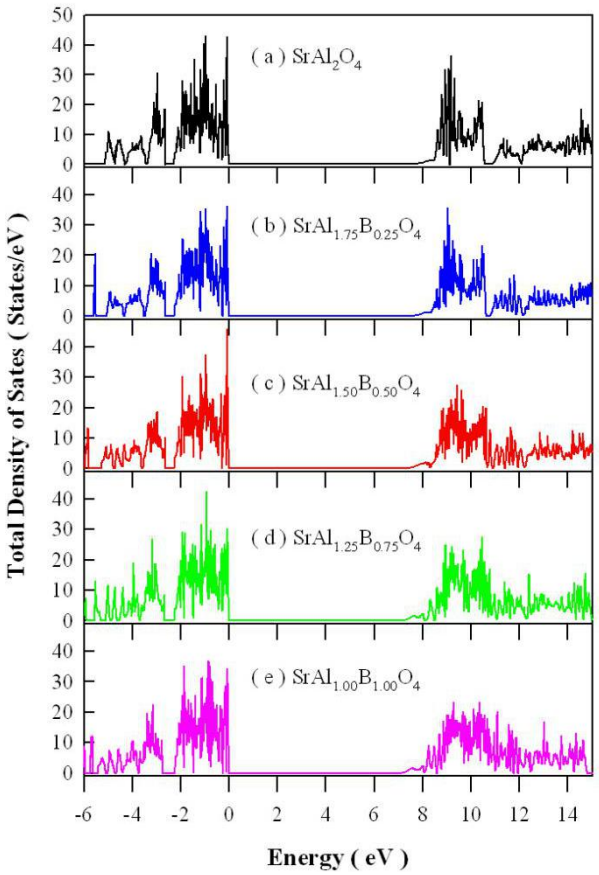

Fig. 5 Calculated densities of states of $SrAl_2O_4$ (*a*), $SrAl_{1.75}B_{0.25}O_4$ (*b*), $SrAl_{1.50}B_{0.50}O_4$ (*c*), $SrAl_{1.25}B_{0.75}O_4$ (*d*), $SrAl_{1.00}B_{1.00}O_4$ (*e*).

4. Conclusions

The impacts of the addition of different amount of H_3BO_3 into the starting material on the crystal structure, photoluminescence and electronic structures of DSAO are investigated. It is found that the crystal structure of

DSAO evolves with the concentration of H_3BO_3 in the starting material. XRD analysis shows that the increase of H_3BO_3 concentration caused the contraction of the unit cell. The addition of different amount of H_3BO_3 has limited effects on the photoluminescent properties and electronic structures of DSAO.

Acknowledgment

This work was financially supported by Natural Science Foundation of China under the Grant No 11574036.

References

[1] Y.M. Huang, Q.L. Ma, Long afterglow of trivalent dysprosium doped strontium aluminate. *J. Lumin.* **160** (2015) 271–275.

[2] Q.L. Ma, B.G. Zhai, Y.M. Huang, Effect of sol-gel combustion temperature on the luminescent properties of trivalent Dy doped $SrAl_2O_4$. *Ceram. Int.* **41** (2015) 5830–5835.

[3] B.G. Zhai, Q.L. Ma, Y.M. Huang, Combustion synthesis and luminescent properties of Eu^{3+} and Dy^{3+} co-doped amorphous $SrAl_2O_4$. *Key Eng. Mater*. **538** (2013) 58–62.

[4] B.G. Zhai, L. Yang, Q.L. Ma, X. Liu, Y,M. Huang, Mechanism of the prolongation of the green afterglow of $SrAl_2O_4$:Dy^{3+} caused by the use of H_3BO_3 flux. *J. Lumin*. **181** (2017) 78–87.

[5] Q.L. Ma, B.G. Zhai, Y.M. Huang, Dopant concentration dependent photoluminescence and afterglow of $SrAl_2O_4$:Dy^{3+} phosphors. *Mater. Res. Innovations* **19** (2015) s40–s44 (2015).

[6] I.C. Chen, T.M. Chen, Sol-gel synthesis and the effect of boron addition on the phosphorescent properties of $SrAl_2O_4$:Eu^{2+},Dy^{3+} phosphors. *J. Mater. Res*. **16** (2001) 644–651.

[7] Y.T. Yu, B.G. Kim, Effects of adding B_2O_3 as a flux on phosphorescent properties in synthesis of $SrAl_2O_4$:(Eu^{2+}, Dy^{3+}) phosphor. *Korean J. Chem. Eng.* **20** (2003) 973–976.

[8] A. Nag, T.R.N. Kutty, Role of B_2O_3 on the phase stability and long phosphorescence of $SrAl_2O_4$:Eu, Dy. *J. Alloy. Compd*. **354** (2003) 221–231.

[9] S. Yoon, J. Bierwagen, M. Trottmann, B. Walfort, N. Gartmann, A. Weidenkaff, H. Hagemann, S. Pokrant, The influence of boric acid on improved persistentluminescence and thermal oxidation resistance of $SrAl_2O_4$:Eu^{2+}. *J. Lumin.* **167** (2015) 126–131.

[10] D. Haranath, P. Sharma, H. Chander, Optimization of boric acid content in developing efficient blue emitting, long persistent phosphor. *J. Phys. D Appl. Phys.* **38** (2005) 371–375.

[11] F. Tran, P. Blaha, Accurate band gaps of semiconductors and insulators with a semilocal exchange-correlation potential. *Phys. Rev. Lett.* **102** (2009) 226401.

[12] D. Koller, F. Tran, P. Blaha, Merits and limits of the modified Becke-Johnson exchange potential. *Phys. Rev. B* **83** (2011) 195134.

[13] A. Balakrishna, O.M. Ntwaeaborwa, Study of luminescent behavior and crystal defects of different $MNa[PO_4]$:Dy^{3+} phosphors (M = Mg, Ca, Sr and Ba). *Sensor. Actuat. B* **242** (2017) 305–317.

[14] B.G. Zhai, L. Yang, Q.L. Ma, Y. M. Huang, First-principles calculations of band structures and optical properties of hexagonal ZnO by using meta-GGA in the framework of density functional theory. *Optoelectron. Mater.* **1** (2016) 13–17.

[15] B.G. Zhai, C. Tang, Y.M. Huang, First-principles density functional calculations of the band structures of $SrAl_2O_4$. *Optoelectron. Mater*. **1** (2016) 18–21.

[16] B.G. Zhai, L. Yang, J.S. Li, Y.M. Huang, Density functional calculations on the electronic structures of triclinic $ZnMoO_4$. *Optoelectron. Mater*. **1** (2016) 43–49.

[17] B.G. Zhai, Y.M. Huang, Effect of post sintering temperature on the morphology and photoluminescence of co-precipitation derived $ZnMoO_4$ microcrystals. *Optoelectron. Mater*. **1** (2016) 50–56.